Charge Transfer Cross Sections for Multiply Charged Slow Ne, Ar, Kr and Xe Ions on Various Gas Targets II. Molecular Gas Targets

By

Hirofumi HANAKI*, Toshio KUSAKABE**, Tadahiko HORIUCHI*, Ichiro KONOMI*, Nobuo NAGAI*, Toru YAMAUCHI* and Masakatsu SAKISAKA*

(Received December 12, 1983)

Abstract

Observed charge transfer cross sections are compiled, similarly to Part I, for multiply charged Ne, Ar, Kr and Xe ions on several molecular targets in an energy region from a few to tens keV. The projectiles are recoil ions produced by using our "ion-impact ion source" (IIIS). The values are compared with the results of other research workers.

1. Introduction

Studies of charge transfer collisions have been intensively carried out in recent years since various information about fundamental processes in a hot plasma can be obtained, something which is necessary to achieve a fusion reactor in the future. In particular, electron captures by multiply charged and slow ions draw attention from the point of fusion engineering because of their quite large cross sections for target atoms and molecules. These play an important role in the energy balance of plasma[1]. The collisions are also interesting processes in the fields of atomic physics, chemistry, radiation physics and astrophysics[2].

In Part I[3] of the previous paper, the authors reported a compilation of charge transfer cross sections for the systems of [Ne^{q+}, Ar^{q+}, Kr^{q+} ions on He] and [Kr^{q+}, Xe^{q+} ions on Ne, Ar, Kr, Xe], where q is the projectile ionicity and the impact energies are chosen from a few to several tens keV. These measurements have revealed the following remarkable facts.

Firstly, the one-electron capture cross sections, $\sigma_{q,q-1}$, show oscillating behaviors

* Department of Nuclear Engineering.
** Department of Nuclear Reactor Engineering, Kinki University, Kowakae, Higashi-osaka.
† Permanent address: Injector Division of Photon Factory, National Laboratory for High Energy Physics, Tsukuba.

against the initial ionic charge q. This is consistent with the prediction of the "classical one electron model" (COEM) of Ryufuku *et al*[4]. Also the cross section magnitudes approximately satisfy a scaling law[5] of $\sigma_{q,q-1} \propto qI^{-2}$, where I is the first ionization potential of target atom. Secondly the multiple-electron transfer cross sections, $\sigma_{q,q-k}$ ($k=1, 2, \cdots$), for Kr^{q+} and Xe^{q+} ions on Ar, Kr and Xe atoms behave very similarly irrespective of the target atom, where k is the number of captured electrons. These σ behaviors against q and k cannot be explained by the "classical absorbing sphere model" (CASM) of Janev *et al*[6]., whereas our "statistical electron transfer model" (SETM)[7] has shown a fairly reasonable accordance. Therefore, it would be very interesting to measure the $\sigma_{q,q-k}$ values for the same ions on various molecular gas targets in the same energy region.

This report is a compilation of these cross sections. As the targets, molecular hydrogen (H_2), molecular nitrogen (N_2), carbon dioxide (CO_2) and three hydrocarbons (CH_4, C_2H_6, C_3H_8) are selected. Table 1 shows the projectile-target combinations and the collision energies.

Table 1. Combination of projectile-target in charge transfer experiment.

Projectile		Collision energy	Target molecule
Ion	Charge q		
Ne^{q+}	2～ 5	1.5 q−12 q keV	H_2
Ar^{q+}	2～ 7	11.4 keV (0.286 keV/amu)	H_2
Kr^{q+}	2～ 9	24 keV (0.286 keV/amu)	H_2, N_2, CO_2, CH_4, C_2H_6, C_3H_8
Xe^{q+}	2～11*	37.6 keV (0.286 keV/amu)	H_2, N_2, CO_2, CH_4, C_2H_6, C_3H_8

* The Xe^{2+}-target combinations, except for the case of Xe^{2+}-H_2, were measured at about 34.5 keV in energy (0.262 keV/amu) to prevent an electrical breakdown in ion acceleration.

2. Experimental

The experimental arrangement is the same as described previously[3]. (See Fig. 1, Part I) Charge-, mass- and energy-filtered heavy ions were introduced into a gas cell to make charge transfer collisions with gas molecules. The charges of the outgoing ions were separated in an electrostatic deflector and hit on a position sensitive detector (PSD). In contrast to the previous detector, the present one was composed of a new 3-stage type microchannel plate* (MCP). This MCP had a better pulse height distribution than before, thus being easier to adjust a lower discrimination level of the SCA connected with the PSD analog processor[8].

Each charge spectrum at a given target thickness was once displayed on a multichannel PHA and then stored in a computer. The charge fraction data obtained

* Specially manufactured by Hamamatsu TV Co., Ltd. The gain is more than 10^8.

as a function of the target thickness were processed by applying a growth rate method. In this way, the cross section values for single- to multiple-electron transfers were derived. Their final errors were evaluated by introducing systematic uncertainties, which are listed in Table 2. These procedures are the same as mentioned in Part I.

Since half of the present apparatus was a charge/mass filter, there existed unavoidable contaminative ions as follows: (O^{4+} and C^{3+} in $^{20}Ne^{5+}$), (O^{2+} in Ar^{5+}), (OH^+ and O^+ in Kr^{5+} and Xe^{8+}), (N^+ in Kr^{6+} and Xe^{9+}), (C^+ in Kr^{7+} and Xe^{11+}) and (O_2^+ in Xe^{4+}). In most cases, the σ values were little affected by these ion impurities, the contributions of which are shown in Table 2. However, a large amount of contaminative C^+ ions was found in Xe^{11+} ions, and the contribution was estimated in each collision by considering the one-electron capture cross section $\sigma_{1,0}$ for C^+-H_2, -N_2, ⋯ or -C_3H_8 collision. As the result, the statistical deviations of the $\sigma_{11,11-k}$ values for Xe^{11+} ions were somewhat larger than others.

Table 2. List of systematic uncertainties.

Origin	Uncertainty (%)
Measurements of gas pressure	7
Effective collision length	5
Temperature	3
Target gas impurity	5
Ion impurity*	<5 for Kr^{5+-7+}
	4 for Ar^{5+}
	3 for $Xe^{8+,9+}$
	2 for Xe^{4+}
	<1 for other ions except Xe^{11+}
Charge separation in PSD and error of diving processor	<10 for Xe^{11+}
	<5 for other ions

* The impurity contents in Xe^{11+} ions were estimated to be 24~54%, the contributions of which are taken into account in deriving the cross section values.

3. Results and comparison with other data

The present charge transfer cross sections are given in Tables 3 to 6, and are depicted in Figs. 1 to 14. The values obtained by other research workers are inserted into these figures for the sake of comparison.

3.1. Ne^{q+}(q=2~5) ions on H_2

The energy range adopted is 1.5-12 keV/q, as listed in Table 1, and the σ data together with those of others are plotted in Fig. 1. Our $\sigma_{2,1}$ results are nearly constant in the measured energy range, whereas those of Huber[9] decrease with increasing ion energy, and our $\sigma_{2,0}$ data show a steeply decreasing behavior. These are

Table 3. Charge transfer cross sections for $Ne^{q+}(q=2\sim5)$ ions on H_2.

Ion^{q+}	Target	Energy (keV)	Cross section (cm^2)	
			$\sigma_{q,q-1}$	$\sigma_{q,q-2}$
Ne^{2+}	H_2	3.0	1.58±0.19(−16)	1.44±0.18(−17)
		6.0	1.48±0.21(−16)	8.48±1.13(−18)
		12.0	1.24±0.15(−16)	4.29±0.52(−18)
		24.0	1.16±0.14(−16)	2.54±0.49(−18)
Ne^{3+}	H_2	5.3	2.49±0.29(−15)	7.14±0.90(−17)
		9.0	2.83±0.33(−15)	4.71±0.79(−17)
		18.0	2.45±0.29(−15)	3.54±0.54(−17)
		36.0	1.79±0.21(−15)	2.91±0.67(−17)
Ne^{4+}	H_2	6.0	3.46±0.41(−15)	3.83±0.94(−17)
		12.0	3.44±0.40(−15)	3.60±1.39(−17)
		24.0	3.40±0.40(−15)	3.59±0.67(−17)
		36.0	3.62±0.42(−15)	3.33±1.01(−17)
Ne^{5+}	H_2	15.0	3.24±0.47(−15)	——
		55.0	2.61±0.37(−15)	——

in contrast to the Ne^{3+}-He collision (see Part I) where both the $\sigma_{2,1}$ and $\sigma_{2,0}$ results sharply increase against impact energy. In Table 3 are given our σ values.

The present $\sigma_{3,2}$, $\sigma_{4,3}$ and $\sigma_{5,4}$ data show gentle behaviors against collision energy and are in general accordance with those of Huber[9]. However, they are smaller than the observations of Salzborn and Müller[10] by 20 to 50% in magnitudes.

3.2. $Ar^{q+}(q=2\sim7)$, $Kr^{q+}(q=2\sim9)$ and $Xe^{q+}(q=2\sim11)$ ions on H_2

The observed cross sections for single- and double-electron transfer at 0.286 keV/amu in impact energy are listed in Table 4 and also illustrated in Figs. 2, 3 and 4 for Ar^{q+}, Kr^{q+} and Xe^{q+} ions on H_2, respectively. The measurements by other workers are inserted into the figures for the sake of comparison.

Our $\sigma_{q,q-1}$ results for Ar^{q+} ions are generally in agreement with those of Salzborn[10] (at 30 keV), Bliman[11] (mean values from $2q$ to $10q$ keV), Crandall[12] (from 10 to 200 keV) and Huber[9,13] (at ~5 keV and other energies) for $q\geq3$. The present $\sigma_{q,q-2}$ values are also consistent with those of Bliman[11] and Huber[13] for $3\leq q\leq5$, whereas discrepancies are seen for $q=6$ and 7. The large deviations for $q=2$ may be explained by a strong energy dependence of both the $\sigma_{2,1}$ and $\sigma_{2,0}$ results. (Refer to Fig. 1.)

The Kr^{q+}-H_2 data are compared in Fig. 3 and a general agreement with the observations of Huber *et al*[13]. (1-10 keV) is seen for $q\geq4$. The disagreement for $q=2$ and 3 can be also attributable to an impact energy dependence of the cross sections.

Figure 4 represents the Xe^{q+}-H_2 case. Our $\sigma_{q,q-1}$ observations are in accordance

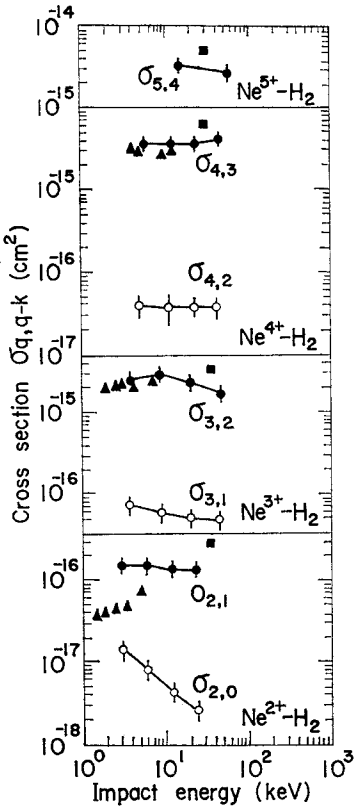

Fig. 1. Charge transfer cross sections for 1.5−12 keV/q Ne^{q+}(q=2∼5) ions on H_2. Solid and open marks stand for $\sigma_{q,q-1}$ and $\sigma_{q,q-2}$, respectively. ●, ○ : present Kyoto, ▲ : Huber[9], ■ : Salzborn and Müller[10].

with those of Crandall *et al*[12]. (near 37.6 keV) for $q \geq 4$, but again show a systematic underestimation from the data of Salzborn[10]. The present $\sigma_{q,q-2}$ results are original, and hence cannot be compared with others.

It is very interesting to note that, when three collisions are compared, the $\sigma_{q,q-1}$ and $\sigma_{q,q-2}$ values against q behave quite similarly, and in particular, the $\sigma_{q,q-2}$ results have maxima at around q=5. This trend should be referred to the Ar^{q+}, Kr^{q+}, Xe^{q+}-He cases. (See Figs. 5∼7, Part I.) Therefore, an important factor can be deduced, namely that three projectiles act like an identical ion having q electron holes, and pick up one or two electrons from a hydrogen molecule similarly.

3.3. Kr^{q+}(q=2∼9) ions on N_2, CO_2, CH_4, C_2H_6 and C_3H_8

In Part I, we have already presented the single- to multiple-electron transfer cross sections for Kr^{q+} ions on the rare gas targets of Ne, Ar, Kr, and Xe, and

Table 4. Charge transfer cross sections for $Ar^{q+}(q=2\sim7)$, $Kr^{q+}(q=2\sim9)$ and $Xe^{q+}(q=2\sim11)$ ions on H_2 at 0.286 keV/amu in energy.

Ion	q	Target	Cross section (cm^2)	
			$\sigma_{q,q-1}$	$\sigma_{q,q-2}$
Ar^{q+}	2	H_2	4.06±0.58(−16)	3.49±0.49(−17)
	3		1.56±0.18(−15)	1.58±0.18(−16)
	4		3.80±0.45(−15)	6.53±0.82(−16)
	5		3.82±0.49(−15)	9.93±1.29(−16)
	6		5.59±0.69(−15)	5.66±0.93(−16)
	7		7.16±0.89(−15)	4.46±0.80(−16)
Kr^{q+}	2	H_2	6.09±0.72(−16)	6.61±1.10(−17)
	3		6.79±0.80(−16)	2.13±0.25(−16)
	4		4.10±0.54(−15)	9.42±1.16(−16)
	5		3.41±0.45(−15)	1.03±0.16(−15)
	6		4.22±0.59(−15)	1.06±0.16(−15)
	7		6.33±0.82(−15)	6.28±0.89(−16)
	8		6.51±0.76(−15)	4.48±0.71(−16)
	9		7.86±1.08(−15)	4.54±1.67(−16)
Xe^{q+}	2	H_2	1.52±0.18(−15)	1.84±0.78(−17)
	3		8.10±0.99(−16)	1.04±0.16(−16)
	4		3.22±0.39(−15)	4.90±0.59(−16)
	5		3.89±0.46(−15)	1.52±0.22(−15)
	6		4.20±0.50(−15)	1.29±0.19(−15)
	7		6.25±0.77(−15)	1.11±0.14(−15)
	8		5.88±0.68(−15)	5.57±0.76(−16)
	9		8.84±1.30(−15)	3.30±0.82(−16)
	10		9.55±1.14(−15)	3.03±1.03(−16)
	11		1.11±0.16(−14)	1.85±0.27(−16)

revealed that these σ values against q show similar statistical patterns. Consequently, we have proposed the "statistical electron transfer model" (SETM)[7] and have obtained a reasonable accordance with the observations. To examine the validity of our model, the charge transfers in the cases of other multi-electron targets should be measured.

The data of Kr^{q+} ions on N_2, CO_2, CH_4, C_2H_6 and C_3H_8 gases are listed in Table 5, and are depicted in Figs. 5, 6, 7, 8 and 9, respectively. These measurements are quite original since the experiments for heavy ions onto molecules are quite poor. Here we mention that there have been published only the $\sigma_{q,q-1}$ results of Salzborn and Müller[10] for the Ar^{q+}-N_2, -O_2, -CO_2 and -CH_4 collisions.

The present $\sigma_{q,q-1}$ values increase with oscillation as the initial charge state q increases. However, the oscillation amplitude becomes smaller as the target molecule

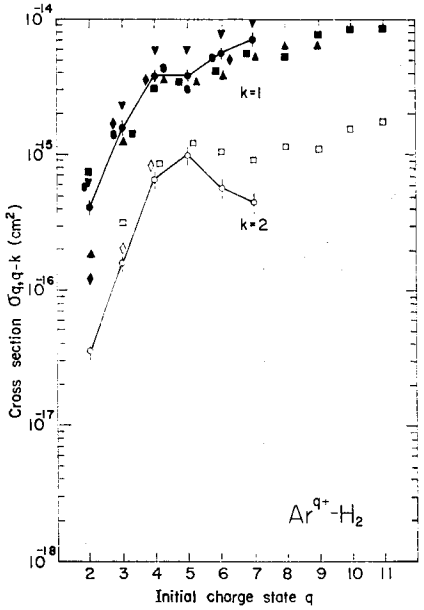

Fig. 2. Charge transfer cross sections for 0.286 keV/amu Ar^{q+}(q=2~7) ions on H_2. Solid and open symbos denote single- and double-electron transfers, respectively. Solid lines are drawn to guide the eye. ●, ○ : present Kyoto, ■, □ : Bliman *et al.*[11], ▼ : Salzborn and Müller, ▲ : Crandall *et al.*[12] The $\sigma_{q,q-1}$ (q=2~8) values are measured from 10 to 200 keV. ◆, ◇ : Huber *et al.*[13], ⬮ : Huber[9]. The values (q=2~6) are obtained at around 2.2 keV/q in energy.

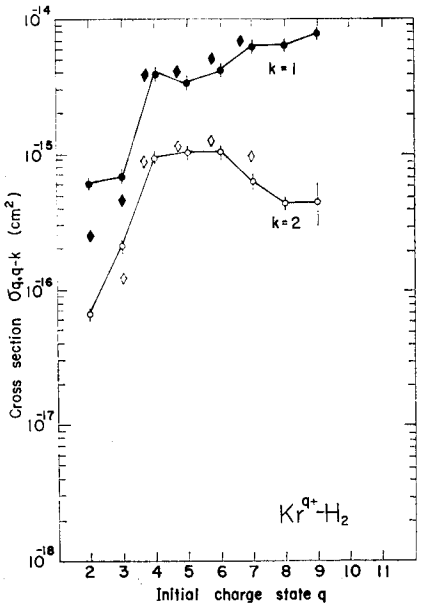

Fig. 3. Charge transfer cross sections for 0.286 keV/amu Kr^{q+}(q=2 ~ 9) ions on H_2. For symbols and lines, see Fig. 2.

becomes more complicated to have a smaller ionization potential. This is consistent with the COEM prediction of Ryufuku *et al*[4]. Our $\sigma_{q,q-k}$ ($k \geq 2$) results gradually change as the molecular complexity proceeds. In fact, those of double- to quadruple-electron captures from C_2H_6 and C_3H_8 become close for high q states. These complicated behaviors may be qualitatively explained as follows:

The constituent interatomic distances in these molecules are large. Hence, a multiple-electron transfer will occur when the projectile passes through a part of such a large molecule——the component molecule would be an effective target, which still consists of a few atoms. Then, the $\sigma_{q,q-k}$ results against q and k show complicated patterns, but the statistical trend is held because of many electrons in the target molecule.

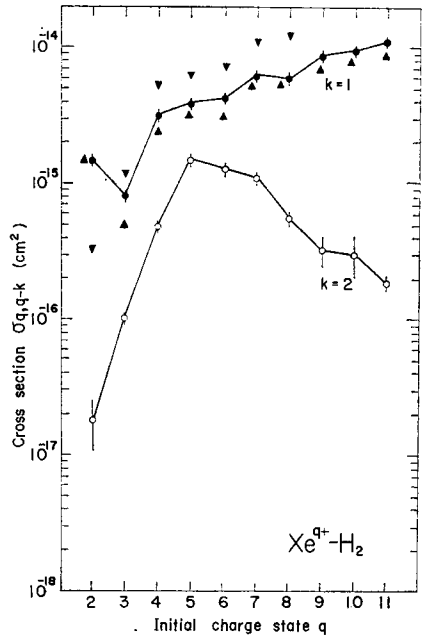

Fig. 4. Charge transfer cross sections for 0.286 keV/amu Xe^{q+}(q=2~11) ions on H_2. For symbols and lines, see Fig. 2. The $\sigma_{q,q-1}$ results by Crandall *et al.* (▲) are obtained at 20.4 to 40.8 keV in energy for q=2 to 10, respectively.

The explanation of the $\sigma_{q,q-k}$'s applying our SETM would be interesting, and we propose the expression for the instance of C_2H_6 as follows:

$$\sigma_{q,q-k}(C_2H_6) = 2 \cdot \sigma_{q,q-k}(CH_3)$$
$$= 2 \sum_{i+j=k} \int_0^\infty 2\pi b \cdot db \cdot {}_mC_i \cdot P_1{}^i(1-P_1)^{m-i} \times {}_nC_j \cdot P_2{}^j(1-P_2)^{n-j}$$

where P_1 and P_2 are the one-electron capture probabilities for C and H_3, respectively, as the functions of the impact parameter b and the projectile charge q. The notations ${}_mC_i$ and ${}_nC_j$ are the binomial coefficients, m and n are the numbers of effectively identical electrons in the clouds of C and H_3, respectively, and $i+j=k$ should be satisfied. Then, the statistics are complicatedly mixed for a given q-k combination according to the P's behaviors. The above formula is our revised proposal, and the applicability will be done elsewhere.

3.4. Xe^{q+}(q=2~11) ions on N_2, CO_2, CO_2 CH_4, C_2H_6 and C_3H_8

The cross sections values for Xe^{q+} ions on the same molecules at the same impact velocity as above are given in Table 6, and are depicted in Figs. 10 to 14.

The oscillating and increasing behaviors of the $\sigma_{q,q-1}$'s as a function of q are again found similarly to the preceding Kr^{q+}-molecule collisions. This is qualitatively

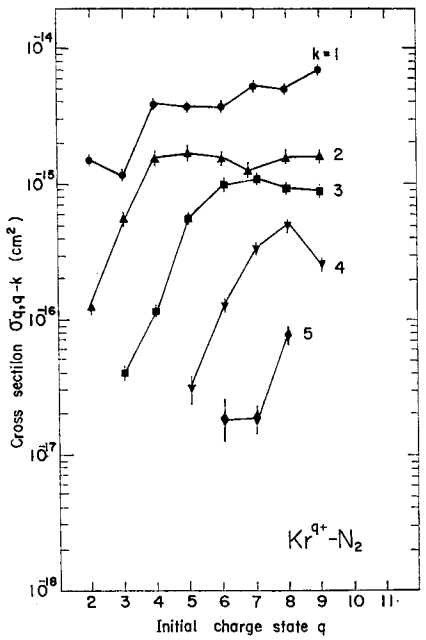

Fig. 5. Charge transfer cross sections for 0.286 keV/amu Kr^{q+}(q=2~9) ions on N_2. The notation k means the number of transferred electrons. Solid lines are served to guide the eye. The marks of ●, ▲, ■, ▼ and ◆ correspond to k=1, 2, 3, 4 and 5, respectively.

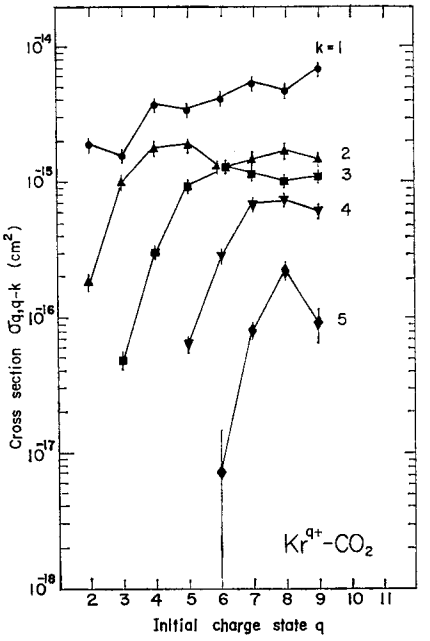

Fig. 6. Charge transfer cross sections for 0.286 keV/amu Kr^{q+}(q=2~9) ions on CO_2. For symbols, see Fig. 5.

and quantitatively supported by the COEM. The $\sigma_{q,q-k}$ results for $k \geq 2$ become closer and more complicated as the molecular weight and the ionicity q increase, and these trends are similar to the Kr^{q+} cases. However, a little difference is seen at around q=9, if we compare the Kr^{q+}-CO_2 collision with that of Xe^{q+}-CO_2 collision, for one example. This is attributable to a shell effect of the projectile ion whereby Kr^{8+} is a closed ion for shell electrons, while Xe^{8+} is a less closed one owing to its electronic complexity. The one-electron capture probability $P(b)$ for the Kr^{q+} ion decreases at around q=9, but that for the Xe^{q+} ion does not drop so significantly. Since the cross section $\sigma_{q,q-k}$ is expressed by our SETM formula, the difference between Kr^{q+} and Xe^{q+} ions appears at around q=9 for the large k values.

4. Summary

We have measured the cross sections of single- to multiple-electron transfers for slow and multiply charged Ne, Ar, Kr and Xe ions on the molecular targets of H_2,

Table 5. Charge transfer cross sections for $Kr^{q+}(q=2\sim9)$ ions on

Ion	q	Target	Cross $\sigma_{q,q-1}$	$\sigma_{q,q-2}$
Kr^{q+}	2	N_2	1.50±0.17(−15)	1.24±0.21(−16)
	3		1.13±0.13(−15)	5.51±0.64(−16)
	4		3.87±0.45(−15)	1.54±0.18(−15)
	5		3.64±0.46(−15)	1.67±0.22(−15)
	9		3.63±0.46(−15)	1.53±0.19(−15)
	7		5.23±0.67(−15)	1.24±0.16(−15)
	8		4.94±0.57(−15)	1.55±0.18(−15)
	9		6.97±0.81(−15)	1.59±0.20(−15)
Kr^{q+}	2	CO_2	1.94±0.23(−15)	1.86±0.27(−16)
	3		1.59±0.19(−15)	1.01±0.12(−15)
	4		3.86±0.45(−15)	1.81±0.21(−15)
	5		3.50±0.44(−15)	1.92±0.24(−15)
	6		4.23±0.54(−15)	1.36±0.18(−15)
	7		5.55±0.71(−15)	1.51±0.20(−15)
	8		4.86±0.57(−15)	1.74±0.20(−15)
	9		7.22±0.84(−15)	1.51±0.20(−15)
Kr^{q+}	2	CH_4	1.34±0.19(−15)	4.57±0.67(−16)
	3		2.00±0.24(−15)	9.60±1.15(−16)
	4		4.76±0.56(−15)	1.88±0.22(−15)
	5		3.89±0.50(−15)	1.90±0.24(−15)
	6		5.64±0.72(−15)	1.55±0.20(−15)
	7		5.96±0.76(−15)	1.76±0.23(−15)
	8		5.82±0.68(−15)	2.01±0.24(−15)
	9		8.63±1.01(−15)	2.05±0.25(−15)
Kr^{q+}	2	C_2H_6	2.07±0.24(−15)	6.52±0.77(−16)
	3		3.98±0.46(−15)	2.02±0.24(−15)
	4		5.11±0.59(−15)	2.22±0.26(−15)
	5		5.82±0.74(−15)	1.92±0.24(−15)
	6		7.14±0.93(−15)	2.40±0.32(−15)
	7		7.07±0.90(−15)	2.18±0.33(−15)
	8		7.56±0.90(−15)	2.41±0.28(−15)
	9		9.83±1.14(−15)	2.16±0.26(−15)
Kr^{q+}	2	C_3H_8	2.30±0.27(−15)	1.02±0.12(−15)
	3		4.81±0.56(−15)	2.61±0.32(−15)
	4		5.24±0.61(−15)	2.31±0.27(−15)
	5		6.50±0.82(−15)	2.24±0.29(−15)
	6		7.58±0.96(−15)	2.56±0.32(−15)
	7		7.57±0.96(−15)	2.35±0.30(−15)
	8		8.56±1.01(−15)	2.58±0.35(−15)
	9		1.18±0.14(−14)	2.09±0.27(−15)

N_2, CO_2, CH_4, C_2H_6 and C_3H_8 at 0.286 keV/amu in energy.

section (cm^2)

$\sigma_{q,q-3}$	$\sigma_{q,q-4}$	$\sigma_{q,q-5}$
—	—	—
3.93±0.50(−17)	—	—
1.16±0.15(−16)	—	—
5.54±0.71(−16)	3.11±0.80(−17)	—
9.63±1.22(−16)	1.29±0.17(−16)	1.93±0.63(−17)
1.08±0.14(−15)	3.34±0.48(−16)	1.87±0.49(−17)
9.21±1.09(−16)	4.97±0.59(−16)	7.72±1.19(−17)
8.74±1.41(−16)	2.57±0.36(−16)	—
—	—	—
4.98±1.06(−17)	—	—
3.14±0.42(−16)	—	—
9.68±1.23(−16)	6.71±0.99(−17)	—
1.34±0.17(−15)	2.95±0.43(−16)	7.61±7.06(−18)
1.19±0.15(−15)	7.14±0.95(−16)	8.07±1.41(−17)
1.06±0.13(−15)	7.63±0.90(−16)	2.28±0.32(−16)
1.13±0.14(−15)	6.33±0.89(−16)	9.75±3.05(−17)
—	—	—
7.34±1.46(−17)	—	—
4.28±0.51(−16)	9.98±5.71(−18)	—
9.45±1.24(−16)	6.20±0.85(−17)	—
1.32±0.17(−15)	3.47±0.47(−16)	1.22±0.82(−17)
1.23±0.16(−15)	6.40±0.85(−16)	3.69±0.99(−17)
1.19±0.14(−15)	6.10±0.74(−16)	9.98±0.32(−17)
1.37±0.16(−15)	2.43±0.47(−16)	—
—	—	—
1.99±0.35(−16)	—	—
1.12±0.13(−15)	3.45±0.75(−17)	—
1.87±0.24(−15)	4.16±0.59(−16)	1.52±0.90(−17)
1.94±0.25(−15)	1.20±0.16(−15)	9.11±4.47(−17)
1.31±0.17(−15)	1.47±0.19(−15)	4.72±0.64(−16)
1.31±0.17(−15)	1.28±0.17(−15)	7.48±0.92(−16)
1.67±0.23(−15)	1.14±0.15(−15)	4.22±0.68(−16)
—	—	—
4.26±0.80(−16)	—	—
1.71±0.20(−15)	7.09±1.63(−17)	—
2.22±0.29(−15)	7.77±1.02(−16)	6.68±1.29(−17)
1.68±0.21(−15)	1.72±0.23(−15)	3.61±0.51(−16)
1.39±0.20(−15)	1.70±0.22(−15)	9.89±1.29(−16)
1.34±0.19(−15)	1.26±0.18(−15)	1.30±0.22(−15)
1.62±0.21(−15)	1.50±0.20(−15)	1.30±0.17(−15)

Table 6. Charge transfer cross sections for Xe^{q+}(q=2~11) ions on

Ion	q	Target	Cross $\sigma_{q,q-1}$	$\sigma_{q,q-2}$
Xe^{q+}	2*	N_2	2.57±0.30(−15)	2.81±1.02(−17)
	3		1.43±0.17(−15)	2.98±0.37(−16)
	4		3.07±0.38(−15)	1.26±0.15(−15)
	5		4.49±0.53(−15)	2.16±0.25(−15)
	6		4.04±0.51(−15)	1.99±0.23(−15)
	7		5.33±0.66(−15)	1.67±0.20(−15)
	8		4.91±0.87(−15)	1.74±0.24(−15)
	9		7.35±0.90(−15)	1.90±0.23(−15)
	10		6.39±0.78(−15)	1.74±0.21(−15)
	11		9.30±2.53(−15)	1.62±0.47(−15)
Xe^{q+}	2*	CO_2	2.62±0.31(−15)	4.62±1.27(−17)
	3		1.65±0.19(−15)	6.84±0.83(−16)
	4		3.39±0.40(−15)	2.18±0.26(−15)
	5		3.96±0.50(−15)	2.23±0.27(−15)
	6		4.35±0.51(−15)	2.13±0.26(−15)
	7		5.06±0.59(−15)	1.69±0.20(−15)
	8		5.03±0.64(−15)	1.63±0.19(−15)
	9		5.81±0.70(−15)	1.55±0.19(−15)
	10		7.47±0.87(−15)	1.77±0.21(−15)
	11		7.87±1.88(−15)	1.69±0.41(−15)
Xe^{q+}	2*	CH_4	1.58±0.19(−15)	2.24±0.33(−16)
	3		1.80±0.21(−15)	9.05±1.06(−16)
	4		4.82±0.57(−15)	2.12±0.25(−15)
	5		4.13±0.48(−15)	2.30±0.28(−15)
	6		5.31±0.63(−15)	1.81±0.23(−15)
	7		5.62±0.67(−15)	1.82±0.22(−15)
	8		6.14±0.72(−15)	1.90±0.24(−15)
	9		8.00±0.98(−15)	1.84±0.23(−15)
	10		9.92±1.15(−15)	2.27±0.27(−15)
	11		—	—
Xe^{q+}	2*	C_2H_6	2.14±0.25(−15)	8.23±0.98(−16)
	3		2.85±0.33(−15)	2.12±0.27(−15)
	4		5.26±0.62(−15)	2.92±0.34(−15)
	5		5.15±0.61(−15)	2.55±0.31(−15)
	6		6.04±0.94(−15)	2.06±0.24(−15)
	7		5.85±0.72(−15)	2.44±0.30(−15)
	8		5.68±0.70(−15)	2.04±0.25(−15)
	9		8.79±1.06(−15)	2.22±0.27(−15)
	10		1.09±0.13(−14)	2.86±0.34(−15)
	11		1.15±0.19(−14)	3.38±0.56(−15)
Xe^{q+}	2*	C_3H_8	2.63±0.31(−15)	8.93±1.10(−16)
	3		3.90±0.46(−15)	2.81±0.34(−15)
	4		5.63±0.66(−15)	3.07±0.37(−15)
	5		5.50±0.65(−15)	2.36±0.29(−15)
	6		6.97±0.83(−15)	2.26±0.27(−15)
	7		6.70±0.79(−15)	2.58±0.31(−15)
	8		7.17±0.88(−15)	2.51±0.29(−15)
	9		1.05±0.13(−14)	2.46±0.30(−15)
	10		1.09±0.14(−14)	2.89±0.38(−15)
	11		1.05±0.23(−14)	3.00±0.66(−15)

* These collisions were measured at about 0.262 keV/amu in energy to

N_2, CO_2, CH_4, C_2H_6 and C_3H_8 at 0.286 keV/amu in energy.

section (cm^2)		
$\sigma_{q,q-3}$	$\sigma_{q,q-4}$	$\sigma_{q,q-5}$
—	—	—
7.88±1.73(−17)	—	—
3.70±0.58(−17)	—	—
4.08±0.51(−16)	1.08±0.60(−17)	—
9.01±1.05(−16)	3.80±1.54(−17)	8.60±5.92(−18)
1.06±0.13(−15)	2.05±0.28(−16)	1.21±0.45(−17)
1.12±0.16(−15)	3.51±0.59(−16)	3.94±1.10(−17)
1.37±0.17(−15)	3.65±0.47(−16)	4.29±1.33(−17)
1.02±0.12(−15)	2.61±0.33(−16)	5.37±0.90(−17)
1.28±0.33(−15)	3.93±1.43(−16)	1.04±0.95(−16)
—	—	—
2.38±0.71(−17)	—	—
1.38±0.21(−16)	—	—
7.10±0.83(−16)	2.81±2.27(−17)	—
1.29±0.16(−15)	1.21±0.25(−16)	—
1.50±0.18(−15)	5.33±0.76(−16)	6.80±0.94(−17)
1.35±0.16(−15)	6.37±0.75(−16)	9.54±1.67(−17)
1.39±0.17(−15)	7.04±0.85(−16)	1.01±0.19(−16)
1.25±0.16(−15)	6.48±0.78(−16)	1.70±0.24(−16)
1.38±0.34(−15)	5.96±1.43(−16)	8.96±6.61(−17)
—	—	—
4.15±2.02(−17)	—	—
1.89±0.54(−16)	—	—
8.98±1.20(−16)	5.86±1.27(−17)	—
1.37±0.17(−15)	2.81±0.37(−16)	—
1.58±0.19(−15)	4.08±0.49(−16)	—
1.45±0.18(−15)	6.29±0.82(−16)	3.10±1.89(−17)
1.58±0.20(−15)	5.24±0.74(−16)	6.24±2.66(−17)
1.49±0.19(−15)	3.99±0.49(−16)	6.52±2.40(−17)
—	—	—
—	—	—
1.31±0.33(−16)	—	—
8.83±1.07(−16)	2.45±1.13(−17)	—
1.89±0.22(−15)	2.05±0.31(−16)	3.13±1.58(−17)
2.18±0.25(−15)	9.15±1.14(−16)	7.43±1.40(−17)
1.66±0.21(−15)	1.57±0.19(−15)	3.27±0.77(−16)
1.43±0.17(−15)	1.21±0.14(−15)	5.24±0.69(−16)
1.65±0.20(−15)	1.46±0.19(−15)	5.05±0.63(−16)
1.60±0.20(−15)	1.53±0.27(−15)	6.22±0.73(−16)
1.86±0.32(−15)	1.55±0.30(−15)	6.36±1.46(−16)
—	—	—
1.62±0.38(−16)	—	—
1.44±0.17(−15)	8.83±1.47(−17)	—
2.48±0.29(−15)	5.47±0.64(−16)	1.23±0.22(−16)
2.30±0.27(−15)	1.53±0.18(−15)	1.51±0.19(−16)
1.61±0.19(−15)	2.07±0.24(−15)	7.77±0.95(−16)
1.61±0.20(−15)	1.58±0.19(−15)	1.05±0.14(−15)
1.48±0.22(−15)	1.69±0.22(−15)	1.01±0.14(−15)
1.30±0.20(−15)	1.55±0.24(−15)	1.09±0.16(−15)
1.62±0.34(−15)	1.02±0.27(−15)	1.12±0.26(−15)

prevent an electrical breakdown in ion acceleration.

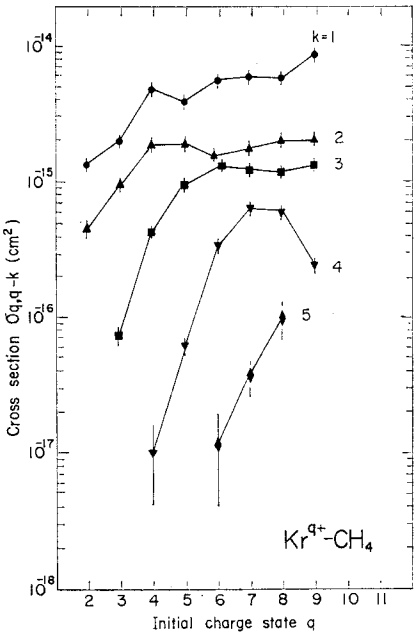

Fig. 7. Charge transfer cross sections for 0.286 keV/amu Kr^{q+}(q=2~9) ions on CH_4.

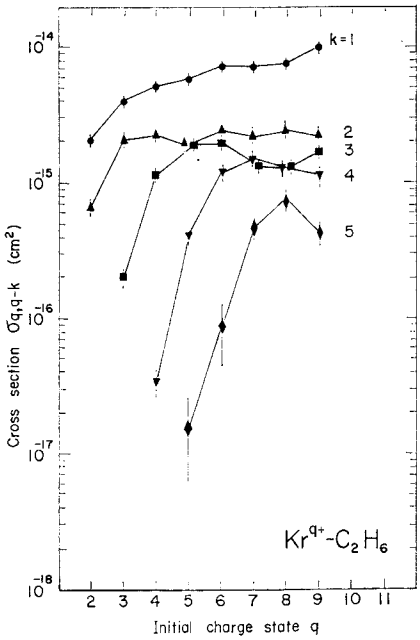

Fig. 8. Charge transfer cross sections for 0.286 keV/amu Kr^{q+}(q=2~9) ions on C_2H_6.

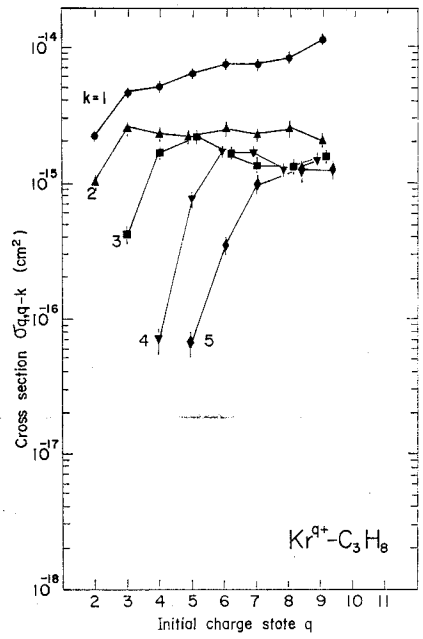

Fig. 9. Charge transfer cross sections for 0.286 keV/amu Kr^{q+}(q=2~9) ions on C_3H_8.

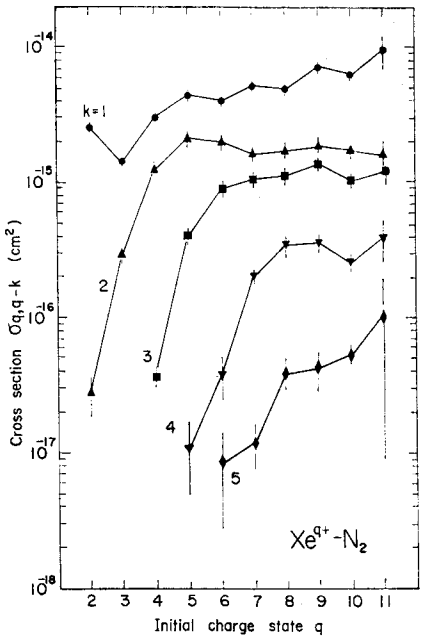

Fig. 10. Charge transfer cross sections for 0.286 keV/amu Xe^{q+}($q=2\sim11$) ions on N_2.

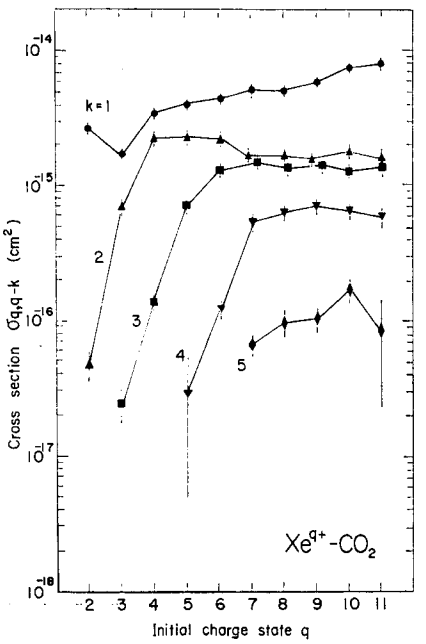

Fig. 11. Charge transfer cross sections for 0.286 keV/amu Xe^{q+}($q=2\sim11$) ions on CO_2.

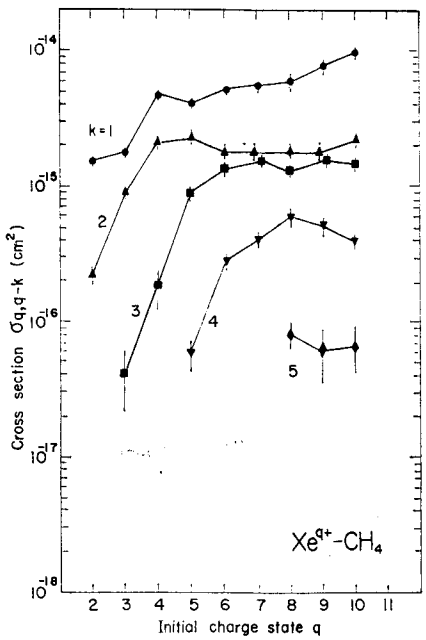

Fig. 12. Charge transfer cross sections for 0.286 keV/amu Xe^{q+}($q=2\sim11$) ions on CH_4.

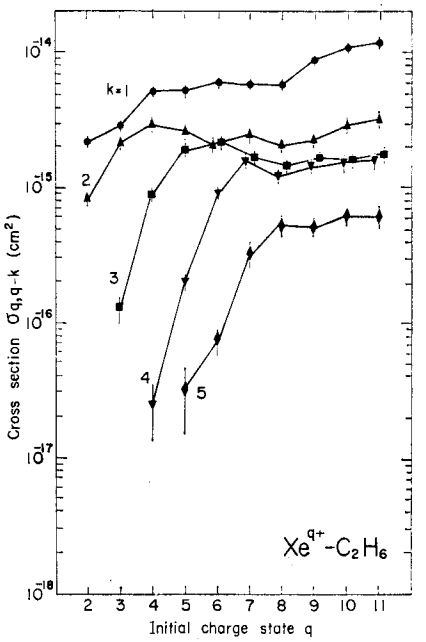

Fig. 13. Charge transfer cross sections for 0.286 keV/amu Xe^{q+}($q=2\sim11$) ions on C_2H_6.

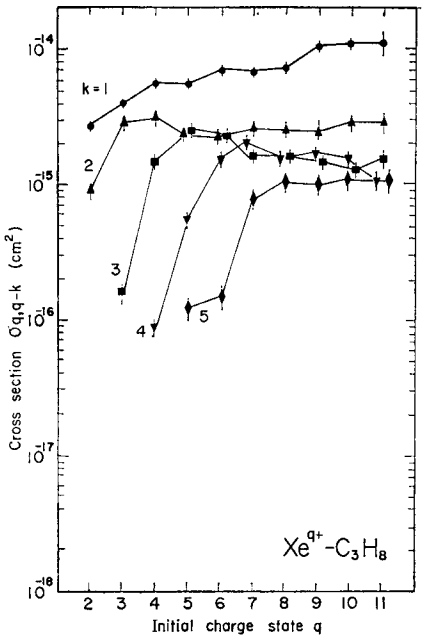

Fig. 14. Charge transfer cross sections for 0.286 keV/amu Xe^{q+}($q=2\sim11$) ions on C_3H_8.

N_2, CO_2, CH_4, C_2H_6 and C_3H_8. These are compiled in " Part II " of this report, and the features are summarized as follows:

(1) The cross sections of the single- and double-electron transfers $\sigma_{2,1}$ and $\sigma_{2,0}$ for Ne^{2+} ions onto H_2 slightly and sharply decrease against impact energy, respectively. These behaviors are in contrast to those for the Ne^{2+}-He collision[3]. (See Part I.)

(2) The double-electron transfer cross sections, $\sigma_{q,q-2}$, for Ar^{q+}, Kr^{q+} and Xe^{q+} ions on H_2 show a very similar dependence on the projectile charge q, and have their maxima at around $q=5$. Note that the maxima in cases using an He target are around $q=7$. (See Part I.)

(3) The single- to multiple-electron transfer cross sections, $\sigma_{q,q-k}$($k=1$, 2, 3, $\cdots$), for Ar^{q+}, Kr^{q+} and Xe^{q+} ions on N_2 to C_3H_8 reveal similar statistical patterns as a function of q, but are more complicated as the target molecule becomes more complex. The statistical behaviors are explained in principle by our " statistical electron transfer model " (SETM)[7].

(4) The $\sigma_{q,q-1}$ values for all targets against the ion charge q show oscillations and increasing magnitudes. This is supported by the prediction of the " classical one electron model " (COEM)[4], and the observed values are consistent with the

calculations by the model.

(5) The present compiled data offer much important information concerning the mechanism of charge transfer collisions, which will be disscussed elsewhere in the near future.

Acknowledgements

The authors would like to express their sincere gratitude to Prof. F. Fukuzawa and Messers T. Tomita, Y. Kanamori and Y. Haruyama for their continuous encouragement and helpful comments. The cooperating efforts of Mr. K. Norizawa for maintaining the laboratory equipment along with the accelerator, and the assistance of Mr. N. Ide for operating various parts of the apparatus are heartfully appreciated. This work was supported by the Scientific Research Expenditure of the Ministry of Education.

References

1) *Proc. Nagoya Semi. on Atomic Processes in Fusion Plasmas*, Nagoya, IPPJ-AM-13 (1978).
2) D. Dalgarno and S. E. Butler; Comm. Atom. Mol. Phys., **7**, 129 (1978).
3) T. Kusakabe, H. Hanaki, N. Nagai, T. Horiuchi, I. Konomi and M. Sakisaka; Mem. Fac. Engng., Kyoto Univ., **45**, 35 (1983).
4) H. Ruyfuku, K. Sasaki and T. Watanabe; Phys. Rev., **A 21**, 745 (1980).
5) T. Kusakabe, H. Hanaki, N. Nagai, T. Horiuchi and M. Sakisaka; Physica Scripta, **T 3**, 191 (1983).
6) R. K. Janev and L. P. Presnyakov; Physics Reports, **70**, 82 (1981).
7) M. Sakisaka, H. Hanaki, N. Nagai, T. Horiuchi, I. Konomi and T. Kusakabe; J. Phys. Soc. Japan, **52**, 716 (1983).
8) H. Hanaki, N. Nagai, T. Kusakabe, T. Horiuchi and M. Sakisaka; Japan. J. Appl. Phys., **22**, 648 (1983).
9) B. A. Huber; Z. Phys., **A 299**, 307 (1981).
10) E. Salzborn and A. Müller; *Electronic and Atomic Collisions*, Invited Papers of the XI-ICPEAC, Kyoto (North-Holland, Amsterdam), p. 407 (1979).
11) S. Bliman, J. Aubert, R. Geller, B. Jacquot and D. Van. Houtte; Phys. Rev. Lett., **46**, 1671 (1981).
12) D. H. Crandall, R. A. Phaneuf and F. W. Meyer; Phys. Rev., **A22**, 379 (1980).
13) B. A. Huber and H. J. Kahlert; J. Phys., **B 13**, L 159 (1980).